




Article

Influence of Co-Precipitation Agent on the Structure, Texture and Catalytic Activity of Au-CeO₂ Catalysts in Low-Temperature Oxidation of Benzyl Alcohol

Lukasz Wolski ^{1,*} , Grzegorz Nowaczyk ² , Stefan Jurga ^{1, 2} and Maria Ziolk ¹ 

¹ Faculty of Chemistry, Adam Mickiewicz University, Uniwersytetu Poznańskiego 8, 61-614 Poznań, Poland; ziolk@amu.edu.pl

² NanoBioMedical Centre, Adam Mickiewicz University, Wszechnicy Piastowskiej 3, 61-614 Poznań, Poland; nowag@amu.edu.pl (G.N.); stjurga@amu.edu.pl (S.J.)

* Correspondence: wolski.lukasz@amu.edu.pl; Tel.: +48-61-829-1794

Abstract: The aim of the study was to establish the influence of a co-precipitation agent (i.e., NaOH—immediate precipitation; hexamethylenetetramine/urea—gradual precipitation and growth of nanostructures) on the properties and catalytic activity of as-synthesized Au-CeO₂ nanocomposites. All catalysts were fully characterized with the use of XRD, nitrogen physisorption, ICP-OES, SEM, HR-TEM, UV-vis, XPS, and tested in low-temperature oxidation of benzyl alcohol as a model oxidation reaction. The results obtained in this study indicated that the type of co-precipitation agent has a significant impact on the growth of gold species. Immediate co-precipitation of Au-CeO₂ nanostructures with the use of NaOH allowed obtainment of considerably smaller and more homogeneous in size gold nanoparticles than those formed by gradual co-precipitation and growth of Au-CeO₂ nanostructures in the presence of hexamethylenetetramine or urea. In the catalytic tests, it was established that the key factor promoting high activity in low-temperature oxidation of benzyl alcohol was size of gold nanoparticles. The highest conversion of the alcohol was observed for the catalyst containing the smallest Au particle size (i.e., Au-CeO₂ nanocomposite prepared with the use of NaOH as a co-precipitation agent).

Keywords: gold; catalysts activity; co-precipitation; one-pot synthesis



Citation: Wolski, L.; Nowaczyk, G.; Jurga, S.; Ziolk, M. Influence of Co-Precipitation Agent on the Structure, Texture and Catalytic Activity of Au-CeO₂ Catalysts in Low-Temperature Oxidation of Benzyl Alcohol. *Catalysts* **2021**, *11*, 641. <https://doi.org/10.3390/catal11050641>

Academic Editor: Werner Oberhauser

Received: 5 May 2021

Accepted: 16 May 2021

Published: 18 May 2021

Publisher's Note: MDPI stays neutral with regard to jurisdictional claims in published maps and institutional affiliations.



Copyright: © 2021 by the authors. Licensee MDPI, Basel, Switzerland. This article is an open access article distributed under the terms and conditions of the Creative Commons Attribution (CC BY) license (<https://creativecommons.org/licenses/by/4.0/>).

1. Introduction

Cerium dioxide is one of the most intensively studied model supports for various metals (e.g., Cu [1–3], Ag [1,4,5], Pt [6] and Au [7,8]). From among numerous ceria-based systems, the catalysts containing gold nanoparticles have attracted particular attention and have been successfully used in different catalytic processes (e.g., Water–Gas Shift reaction [9], oxidation of CO [10,11], alcohols [12–14] and formaldehyde [15]). In terms of selective oxidation of alcohols, it has been established that one of the most important factors affecting the activity and selectivity of Au/CeO₂ catalysts is the size of the supported gold nanoparticles [11,16] and the concentration of lattice defects in the ceria support [17]. These two factors have been considered as the key guidelines on the development of new methods for the synthesis of highly active ceria-based gold catalysts. Literature data show that various strategies to meet these two criteria can be applied, e.g., development of new methods for gold deposition [18–21] or design of new supports by controlling ceria morphology [9,10].

According to literature [22–25], geometric and electronic properties of gold are strongly affected by the type of precipitation agent used during the synthesis of catalysts. Radnik et al. [23] have found that Au/Al₂O₃ catalysts prepared by deposition–precipitation method using two different precipitation agents, namely NaOH and urea, had not only different particle size, but also showed different electronic properties of gold species. In the

catalyst prepared using urea, they observed only metallic gold species, while in the catalyst prepared with the use of sodium hydroxide, they identified two forms of gold, namely metallic gold and partially oxidized gold species. Differences in electronic properties of gold nanoparticles (Au NPs) loaded on TiO₂ surface, using different precipitation agents, have been also observed by Zanella et al. [24]. The authors have found that Au NPs prepared using NaOH as a precipitation agent were more easily reducible than those prepared with the use of urea. The influence of the precipitation agent on the properties and catalytic activity of gold catalysts supported on ceria has also been studied by Chen et al. [25]. The authors have reported that the highest activity in gas phase oxidation of formaldehyde was characteristic of the sample prepared with the use of urea. High activity of this sample was attributed by these authors to smaller gold particle size and stronger metal-support interaction than that observed for the catalyst prepared with the use of sodium hydroxide. Chen et al. [25] have claimed that the efficient charge transfer from gold nanoparticles to ceria support observed for the catalyst prepared with the use of urea resulted in formation of large quantities of Au³⁺ and Ce³⁺ species. According to the same authors, the presence of this strong electronic interaction weakened the Ce-O bonds, leading to easier reduction of the ceria surface oxygen species, and this promoted high activity of this sample in gas phase oxidation of formaldehyde. In view of these results, one can conclude that there is no simple correlation between the type of precipitation agent used during the synthesis and the properties/activity of as-prepared gold species.

Recent literature reports have shown that not only NaOH and urea, but also hexamethylenetetramine (HMTA) can be successfully used for the synthesis of heterogeneous catalysts with desirable properties [26–28]. Similarly to urea, HMTA undergoes hydrolysis at higher temperatures leading to formation of NH₃ [27]. The as-formed ammonia produces a basic environment that is necessary for the production of metal hydroxides, which can be further transformed into relevant metal oxides. To date, HMTA has been successfully used by She et al. [26] for the synthesis of gold catalysts supported on zinc oxide nanorods. These authors have discovered that polyvinylpyrrolidone (PVP)-assisted in situ nucleation and growth of ZnO nanorods in the colloidal solution of gold nanoparticles can lead to successful formation of well-defined nanostructures. A recent report by Saad et al. [29] has shown that HMTA can be used not only for the preparation of ZnO-based materials, but also for the synthesis of Ag-, Al- and Zn-doped TiO₂ nanostructures. One of the most important differences between urea and HMTA is the type of side products of their hydrolysis. As mentioned previously, heating of water solution of urea or HMTA leads to formation of ammonia as the main product. However, hydrolysis of the former precipitation agent leads also to formation of carbon dioxide [30,31], while hydrolysis of the latter precipitation agent results in production of formaldehyde [27]. It is expected that in situ formation of these two different side products during the synthesis of gold catalysts may have significant impact on the growth of nanostructures and properties of as-prepared materials.

The main goal of this work was to establish the influence of the type of co-precipitation agent on the structure, texture, electronic and catalytic properties of Au-CeO₂ catalysts prepared by a facile co-precipitation method. Of particular interest was to identify correlations between the properties of co-precipitation agents used during the synthesis of gold catalysts (NaOH—immediate precipitation of Au-CeO₂ nanostructures vs. HMTA and urea—gradual precipitation and growth of Au-CeO₂ nanostructures) and the properties of as-synthesized Au-CeO₂ nanostructures. The activity of the catalysts was tested in low-temperature oxidation of benzyl alcohol as a model reaction, which allowed identification of correlations between the properties of the as-prepared Au-CeO₂ composites and their catalytic performance.

2. Results

2.1. Characterization of Materials

Chemical composition of Au-CeO₂ catalysts was analyzed using Inductively Coupled Plasma—Optical Emission Spectrometry (ICP-OES; see Table 1). It was found that for

all catalysts synthesized in this study, high efficiency of gold introduction was achieved. The highest gold loading of 4.7 wt. % was characteristic of the catalyst prepared with the use of HMTA as a co-precipitation agent. For the catalysts synthesized with the use of NaOH and urea, the real gold loading was slightly lower and was found to be of 4.5 and 4.3 wt.%, respectively.

Table 1. Characteristics of catalysts prepared with the use of different co-precipitation agents: urea (catalysts labelled as CeO₂_U and Au-CeO₂_U), HMTA (catalysts labelled as CeO₂_H and Au-CeO₂_H) and NaOH (catalysts labelled as CeO₂_N and Au-CeO₂_N).

Catalyst	Real Gold Loading ¹ (wt.%)	BET Surface Area ² (m ² /g)	Average Pore Size ³ (nm)	Average Gold Particle Size ⁴ (nm)
CeO ₂ _U	-	46	6.9	-
Au-CeO ₂ _U	4.3	35	6.5	61.8
CeO ₂ _H	-	11	17.1	-
Au-CeO ₂ _H	4.7	28	12.0	51.5
CeO ₂ _N	-	49	8.1	-
Au-CeO ₂ _N	4.5	45	7.4	12.5

¹ estimated using ICP-OES; ² estimated by Brunauer–Emmett–Teller (BET) method, ³ estimated from adsorption branch using Barrett–Joyner–Halenda (B.J.-H.) method; ⁴ estimated from XRD patterns using the Scherrer equation.

Structure of the materials was analyzed by X-ray diffraction measurements (XRD). It was found that all the catalysts synthesized in this study, irrespectively of the co-precipitation agent used during the synthesis, had cerianite structure (ICDD No. 00-034-0394; see Figure 1). For the gold containing catalysts, four additional diffraction peaks at 2θ equal to 38.2, 44.4, 64.5 and 77.5° were found. According to literature, these diffraction peaks are characteristic of (111), (200), (220) and (311) facets of metallic gold nanoparticles, respectively [32,33].

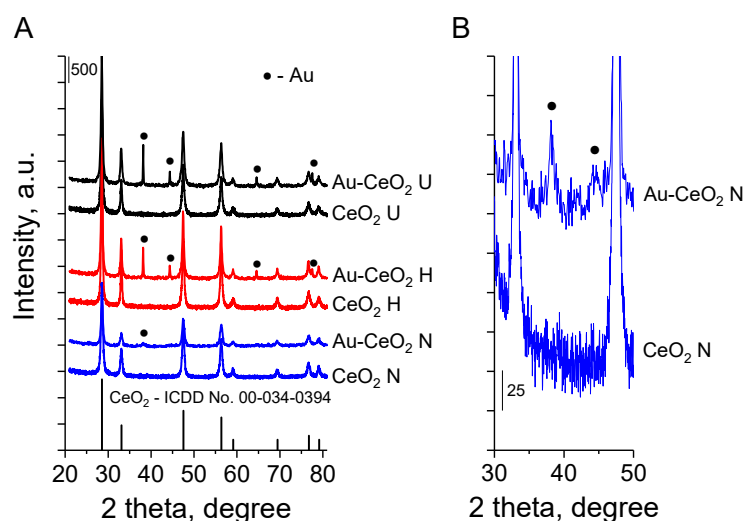


Figure 1. XRD patterns of as-synthesized materials (A) and XRD patterns recorded for materials prepared with the use of sodium hydroxide as a co-precipitation agent shown at higher magnification (B).

As can be seen from Figure 1A, the type of co-precipitation agent had significant impact on the size of gold nanoparticles. For the gold catalysts prepared with the use of urea and HMTA, the diffraction peaks typical of Au NPs were much sharper and more intense than that observed for the catalyst prepared with the use of sodium hydroxide, indicating larger gold particle size for the former two catalysts. The average gold particle sizes estimated from XRD patterns using the Scherrer equation were found to be of 61.8, 51.5 and 12.5 nm for Au-CeO₂_U, Au-CeO₂_H and Au-CeO₂_N, respectively (see Table 1).

Figure 2 shows nitrogen adsorption–desorption isotherms recorded for the catalysts. It was found that all materials exhibited isotherms of type IV(a) characteristic of porous solids [34], but had different surface areas. From among all cerium dioxides synthesized in this study, the highest surface area of $49 \text{ m}^2/\text{g}$ was characteristic of the sample prepared with the use of sodium hydroxide as a co-precipitation agent. The surface area of the ceria support prepared with the use of urea was slightly lower than that observed for $\text{CeO}_2\text{-NaOH}$ ($46 \text{ m}^2/\text{g}$ vs. $49 \text{ m}^2/\text{g}$, respectively), while the lowest surface area of $11 \text{ m}^2/\text{g}$ was characteristic of the ceria catalyst prepared with the use of HMTA (see Table 1).

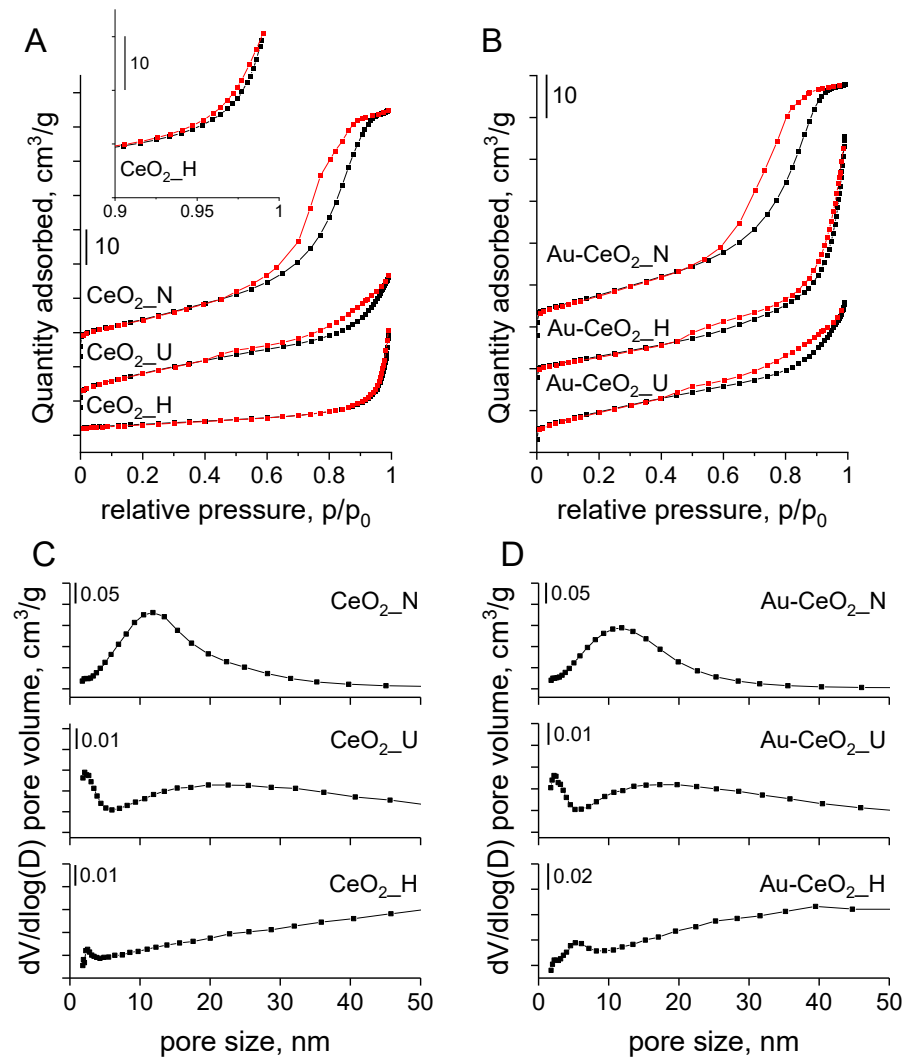


Figure 2. Nitrogen adsorption–desorption isotherms (A,B) and pore size distribution (C,D) estimated for CeO_2 and Au-CeO_2 catalysts.

Detailed analysis of the hysteresis loops permitted us to conclude that the type of co-precipitation agent affected not only the surface area of ceria but also had a significant impact on the pore structure of as-synthesized materials. As can be seen from Figure 2A, $\text{CeO}_2\text{-N}$ catalyst exhibited a hysteresis loop of type H2, while $\text{CeO}_2\text{-H}$ and $\text{CeO}_2\text{-U}$ samples exhibited hysteresis loops of type H3. The H2 hysteresis loop found for $\text{CeO}_2\text{-N}$ may be associated with pore blocking effect and indicated the presence of mesopores with a narrow range of pore necks [34]. On the other hand, hysteresis loop of type H3 found for $\text{CeO}_2\text{-H}$ and $\text{CeO}_2\text{-U}$ indicated the presence of macropores in the structure of these materials. Differences in porosity of ceria catalysts were further confirmed by the pore size distributions (see Figure 2C). It was found that $\text{CeO}_2\text{-N}$ sample contained mesopores of sizes in the range from 2 to 30 nm, while the pore network of $\text{CeO}_2\text{-U}$ and $\text{CeO}_2\text{-H}$

consisted of small mesopores with the size of ca. 2 nm, but some large meso- and even some macropores were also identified.

Figure 2B,D shows that gold catalysts had similar pore structures and pore size distributions as that observed for ceria supports prepared with the use of the same co-precipitation agent. In terms of catalysts surface area, it was found that gold catalysts prepared with the use of NaOH and urea had slightly lower surface areas than that observed for the samples without gold (see Table 1). On the other hand, the surface area of gold catalyst prepared with the use of HMTA was ca. three times higher than that observed for CeO₂_H (28 m²/g vs. 11 m²/g, respectively; Table 1). Detailed analysis of pore size distribution estimated for CeO₂_H and Au-CeO₂_H sample permitted us to observe that the presence of chloroauric acid during the synthesis of materials led to formation of additional mesopores with the sizes in the range from 5 to 10 nm.

Morphology of the catalysts was characterized using the Scanning Electron Microscopy (SEM). As shown in Figure 3, the type of co-precipitation agent had significant impact on the structure of materials obtained. Cerium dioxide prepared with the use of HMTA was composed of irregular aggregates of particles with different shapes, mostly spherical-shape particles.

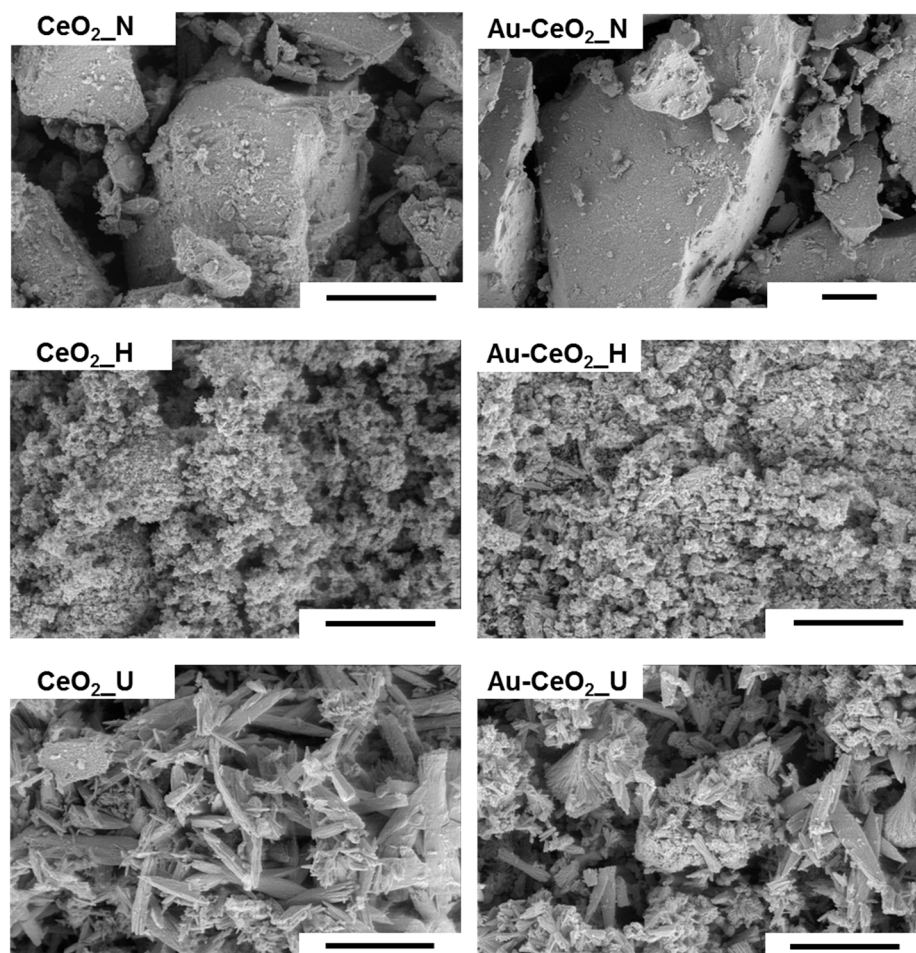


Figure 3. SEM images of catalysts. Scale bars represents 10 μ m.

On the other hand, the catalyst prepared using urea as a co-precipitation agent consisted of strips aggregated into coralloid-like structures. The highest distortions of sizes and shapes of CeO₂ particles were observed for the catalysts prepared with the use of NaOH. As can be seen from Figure 3, CeO₂_N was composed of large irregular aggregates of different shapes and sizes accompanied by smaller and very small irregular nanoparticles.

It is important to notice that all gold catalysts had morphology similar to that of cerium oxides synthesized using the same co-precipitation agents.

To get a deeper insight into the morphology and structure of the materials, the as-prepared catalysts were analyzed with the use of High Resolution Transmission Electron Microscopy (HRTEM). As shown in Figures S1–S3, all cerium oxides consisted of small nearly spherical, highly crystalline particles fused into larger aggregates. It is worth noting that the most condensed structures were observed for the ceria support prepared with the use of urea as a co-precipitation agent (CeO₂_U; see Figure S3). The HRTEM images revealed a characteristic distance of about 3.1 Å for all the samples, attributed to the (111) CeO₂ lattice planes. Further analysis of crystalline parameters calculated on the basis of Selected Area Electron Diffraction (SAED) patterns (Figures S1–S3) showed that they were in good agreement with those obtained from XRD experiments.

Detailed analysis of gold catalysts with the use of HRTEM provided a deeper insight into the role of a co-precipitation agent in controlling the size of gold nanoparticles (see Figure 4). It was found that the smallest and the most homogeneous in size gold nanoparticles were formed with the use of NaOH as a co-precipitation agent. Additionally, with this co-precipitation agent, it was frequently observed that gold particles of single nanometers size were tightly attached to CeO₂ nanoparticles (see inset in Figure 4A). Gold nanoparticles formed in the presence of HMTA were much larger and less homogeneous in size than those observed for Au-CeO₂_N (see Figure 4B). The largest differences in size of gold nanoparticles were noted for the catalyst prepared with the use of urea as a co-precipitation agent. It was found that Au-CeO₂_U catalyst contained both relatively small Au NPs with the size below 15 nm and large gold nanoparticles with the size larger than 30 nm (see Figure 4C). To shed more light on the distribution of gold nanoparticles formed on the surface of the catalysts, the as-prepared materials were further analyzed with the use of Energy Dispersive X-ray Spectroscopy (EDS) combined with elemental mapping. The detailed analysis of EDS maps of elements recorded for Au-CeO₂_N allowed drawing a conclusion that the use of sodium hydroxide as a co-precipitation agent resulted in formation of relatively small and uniform Au NPs (see Figure 5A,A'). TEM-EDS measurements confirmed also large variations in the size of gold species formed in the presence of HMTA as a co-precipitation agent (see Figure 5B'). The greatest diversity in gold particle size was observed for Au-CeO₂_U. For this material, we identified both some gold nanoparticles with the size ranging from 10 to 30 nm (see Figure 5C,C') and extremely large gold aggregates shown in Figure 5 D and D' (the regions containing extremely large gold nanoparticles were very rare). Oxidation state of metals in the catalysts was investigated by the Ultraviolet-visible (UV-vis) spectroscopy. As can be seen from Figure 6, all materials exhibited broad absorption bands with the maximum intensity at ca. 260 and 345 nm. According to literature [35,36], these bands are attributed to O²⁻ → Ce⁴⁺ charge transfer transitions and interband transitions, respectively. It is important to notice that the band at ca. 255 nm corresponding to the O²⁻ → Ce³⁺ charge transfer transitions was not clearly observed in the UV-vis spectra [35,37]. However, it cannot be excluded that this band is overlapped with the more intense absorption bands typical of Ce⁴⁺ species. The presence of Ce³⁺ ions in the structure of ceria supports will be further discussed in the X-ray Photoelectron Spectroscopy (XPS) section. Figure 6B shows that the UV-vis spectra recorded for all gold catalysts exhibited additional absorption band with a maximum intensity at ca. 500–650 nm. According to literature [38,39], this absorption band is assigned to Surface Plasmon Resonance (SPR) of metallic gold nanoparticles. Thus, UV-vis studies provided us further evidence for successful deposition of metallic gold species on the surface of all the catalysts. Furthermore, significant differences in the positions of the SPR bands for Au NPs shown in Figure 6B permitted concluding that the nature of co-precipitation agent strongly affected the optical properties of as-prepared Au-CeO₂ nanocomposites.

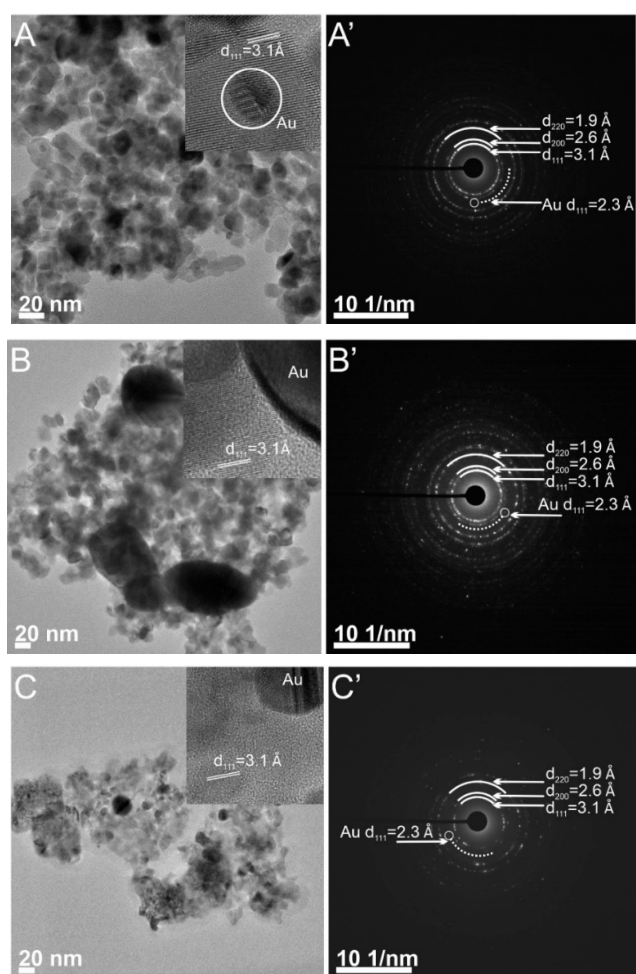


Figure 4. HRTEM images and Selected Area Electron Diffraction (SAED) patterns of Au-CeO₂_N (A,A'), Au-CeO₂_H (B,B') and Au-CeO₂_U (C,C'). The insets in (A–C) show the interplanar distance between the (111) planes of CeO₂ and a single gold particle (dark region).

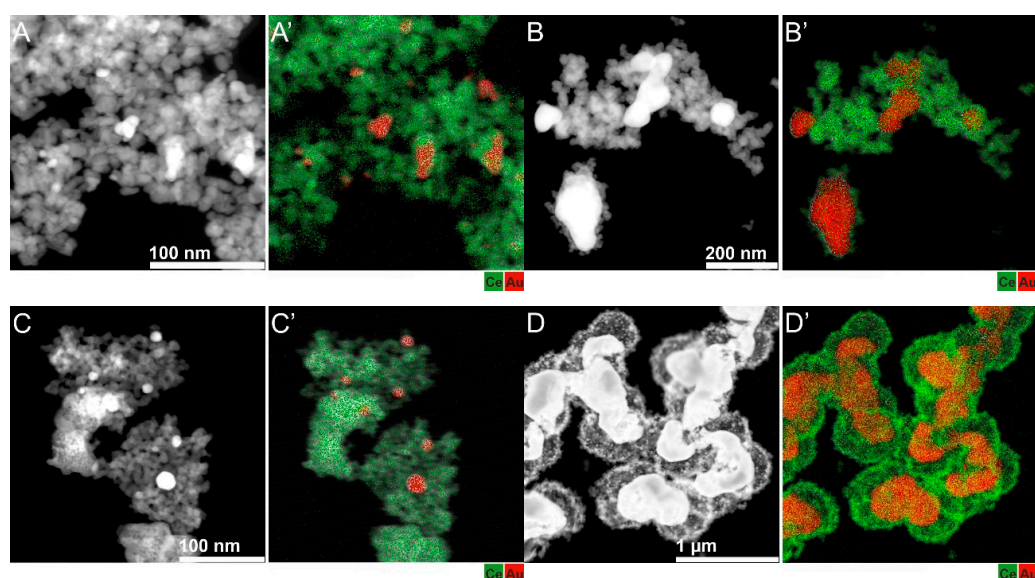


Figure 5. High angle annular dark field STEM (HAADF STEM) image and EDS elemental map of Au-CeO₂_N (A,A'), Au-CeO₂_H (B,B') and Au-CeO₂_U (C,C',D,D').

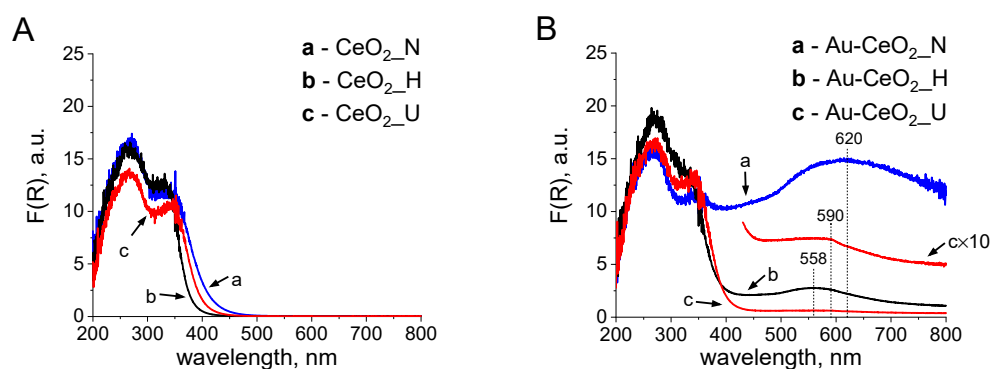


Figure 6. (A,B) Diffuse Reflectance UV-vis spectra of catalysts.

To get a deeper insight into the chemical composition of the catalysts, the samples were further characterized using XPS. Figures 7 and 8 show the Ce 3d and Au 4f XP spectra of all materials. As can be seen from Figure 7A, the type of co-precipitation agent has no significant influence on the oxidation state of ceria.

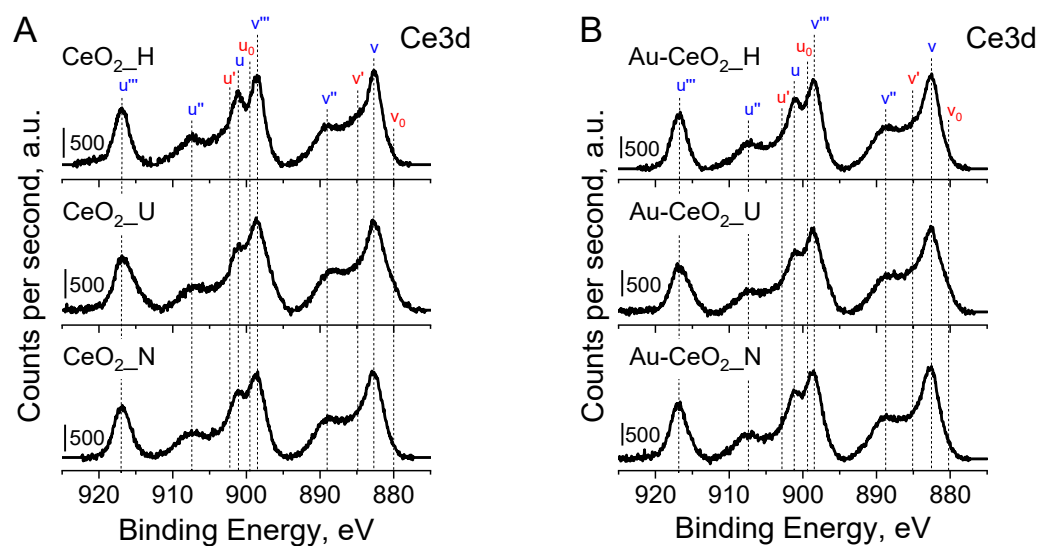


Figure 7. Ce 3d XP spectra of ceria supports (A) and gold catalysts (B).

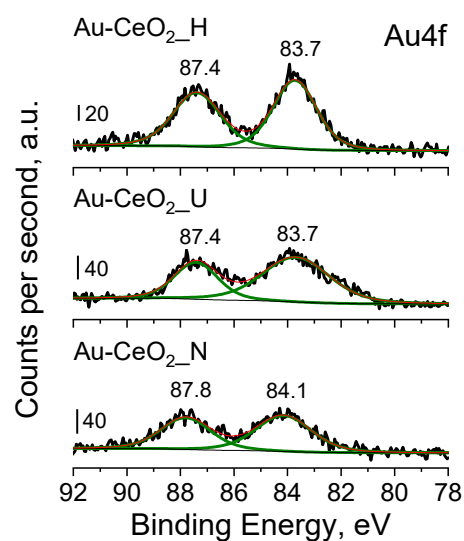


Figure 8. Au 4f XP spectra of catalysts.

In all the samples, the most intense peaks were typical of Ce^{4+} species (labelled as v, v'', v''' and u, u'', u''' [20,40]), indicating that majority of cerium species existed in the form of CeO_2 . The contribution of components typical of Ce^{3+} species or lattice defects (labelled as v_0, v' and u_0, u' [20,40]) in all the samples was noticeable, but significantly lower than that observed for Ce^{4+} species. This observation indicated that some Ce^{3+} species or lattice defects (e.g., oxygen vacancies) can be present in the structure of all the ceria-based catalysts, but the majority of cerium existed as Ce^{4+} .

Important factors affecting the activity of gold catalysts in oxidation reactions are electronic properties of gold. As can be seen from Figure 8, in the Au 4f region of the XP spectra recorded for Au- CeO_2 -N, two spectral components at the binding energy of 84.1 and 87.8 eV, were observed. According to literature, these two components are characteristic of metallic gold species (spin orbitals Au 4f_{7/2} and Au 4f_{5/2}, respectively [41]). For Au- CeO_2 -H and Au- CeO_2 -U, we observed the same components but at lower binding energy values. The shift of BE of the Au 4f spectral components towards lower values may result from larger gold particle size observed for these two catalyst. As mentioned in the XRD and TEM sections, Au NPs formed on the surface of the catalyst prepared with the use of HMTA and urea were much larger than that found on the surface of Au- CeO_2 -N. Thus, in view of all the information, one can observe that the results of XPS studies are in agreement with the conclusions drawn on the basis of XRD and TEM measurements.

2.2. Catalytic Activity

Catalytic activity of the materials was tested in low-temperature oxidation of benzyl alcohol in liquid phase. As implied by Table 2 data, CeO_2 -U and CeO_2 -H exhibited no activity in this process, while as a result of the reaction with the use of CeO_2 -N, traces of benzoic acid were formed. Thus, ceria itself is inactive in this reaction.

Table 2. Results of benzyl alcohol oxidation at 40 °C¹.

Catalyst	Reaction Time [Min]	Conversion [%]	Selectivity [%]	
			Benzaldehyde	Benzoic Acid
CeO_2 -U	40	-	-	-
Au- CeO_2 -U	40	17	56	44
CeO_2 -H	40	-	-	-
Au- CeO_2 -H	20	20	52	48
	40	38	22	78
CeO_2 -N	40	<< 1	-	traces
Au- CeO_2 -N	20	33	14	86
	40	47	9	91

¹ Reaction conditions: catalyst (20 mg), deionized water (10 mL), benzyl alcohol (20 μL), sodium hydroxide (390 μL of 0.5 M water solution of NaOH), oxygen atmosphere (balloon filled with oxygen connected to the reactor), stirring (800 RPM).

Deposition of gold on ceria resulted in a significant increase in the catalysts performance. It means that gold is the active phase in this reaction and the presence of this noble metal is essential for oxidation of the alcohol. The highest activity after 40 min of the reaction was observed for Au- CeO_2 -N (47% of alcohol conversion). Au- CeO_2 -H was less active than Au- CeO_2 -N (47% vs. 38% of alcohol conversion, respectively), while the lowest activity was characteristic of Au- CeO_2 -U (17% of alcohol conversion). To compare the activity of Au- CeO_2 -H and Au- CeO_2 -N at lower conversion of the alcohol the reaction time was reduced by half. As follows from Table 2, after 20 min of the reaction we observed the same tendency as previously described. In a shorter reaction time, Au- CeO_2 -N sample was still more active than Au- CeO_2 -H (33 vs. 20% of benzyl alcohol conversion, respectively). In terms of selectivity, it was established that at a low conversion of benzyl alcohol a significant amount of benzaldehyde was formed. However, with increasing alcohol conversion, the selectivity to benzoic acid increased. From among all the catalysts

the highest selectivity to benzoic acid was shown by Au-CeO₂_N sample (91% of benzoic acid selectivity after 40 min of the reaction).

To get a deeper insight into the oxidation of benzyl alcohol over the most active sample, i.e., Au-CeO₂_N, the additional experiments in different reaction times and temperatures were performed. As can be seen from Figure 9A, the increase in reaction time led to an almost linear increase in the benzyl alcohol conversion. After 120 min of the reaction, Au-CeO₂_N exhibited a very high activity of 98%. It is important to notice that with increasing the reaction time, the selectivity to benzoic acid also grew. According to Figure 9A, after 120 min of the reaction, benzoic acid was the only product. As far as the reaction temperature effect is concerned, it was found that the increase in reaction temperature from 40 °C to 80 °C led to the increase in the alcohol conversion from 47 to 58%, but had negligible impact on the selectivity (see Figure 9B). Au-CeO₂_N exhibited very high selectivity to benzoic acid of ca. 90%, irrespectively of the reaction temperature.

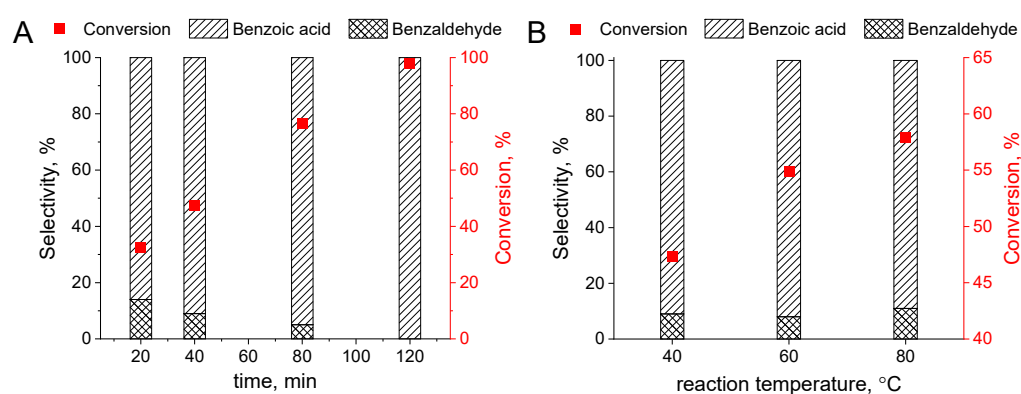


Figure 9. Activity and selectivity of Au-CeO₂_N in benzyl alcohol oxidation after different reaction times at 40 °C (A) and after 40 min of reaction at different temperatures (B).

3. Discussion

Results obtained in this study clearly show that the type of co-precipitation agent has a significant impact on the properties and catalytic activity of gold catalysts supported on cerium dioxide. The highest activity in low-temperature oxidation of benzyl alcohol was observed for the sample prepared with the use of sodium hydroxide as a co-precipitation agent. This catalyst had the highest surface area, the smallest gold particle size and the most uniform gold species. The latter two features of Au-CeO₂_N catalyst resulted most likely from different growth mechanism of the nanostructure. Very important role in this process played different solubility of Au(OH)₃ and Ce(OH)₃ species. According to literature [42], the former species are much less soluble than the latter. As described in the experimental section, during the synthesis of Au-CeO₂_N catalyst, the precipitation of both gold and cerium hydroxides was observed immediately after addition of NaOH because of a very fast increase in pH of the reaction mixture (high excess of NaOH). Under such reaction conditions, gold hydroxides could be adsorbed and stabilized on the surface of the as-formed cerium hydroxides during the hydrothermal treatment, and this promoted formation of small gold nanoparticles of the size of ca. 12.5 nm (see Table 1). In the case of syntheses with the use of HMTA and urea as co-precipitation agents, the concentration of hydroxide anions was very low at the beginning of the syntheses and increased during the gradual hydrolysis of the co-precipitation agents. Under such reaction conditions, gold hydroxides appeared before the cerium hydroxides because of lower solubility of the former species. Under such conditions, the aggregation of gold hydroxides in larger particles was favored, and this resulted in formation of much larger gold nanoparticles with large variations in gold particle size as observed for Au-CeO₂_H and Au-CeO₂_U. In view of the results obtained in this study, one can conclude that future research aiming at the synthesis of new and more active gold catalysts should be performed with the use of strong bases, such as NaOH, which cause immediate co-precipitation of metal ions.

As to the catalysts selectivity, Au-CeO₂_N was observed to show the highest selectivity to benzoic acid. As described in the section on catalytic tests, Au-CeO₂_N exhibited higher selectivity to benzoic at lower conversion of benzyl alcohol than Au-CeO₂_H at a higher conversion of the alcohol (86% of selectivity to benzoic acid at 33% of alcohol conversion for Au-CeO₂_N vs. 78% selectivity to benzoic acid at 38% of alcohol conversion for Au-CeO₂_H, respectively; Table 2). Both catalysts had similar gold loading, but totally different porosity and pore structure. Au-CeO₂_H had not only ca. twice larger average pores than Au-CeO₂_N (12.0 nm vs. 7.4 nm, respectively; Table 1), but also much broader pore size distribution (pore structure of Au-CeO₂_H sample consisted not only of mesopores, but also some macropores; see Figure 2D). Furthermore, SEM images of the catalysts clearly showed that the aggregates of Au-CeO₂_N particles were much larger than those observed for Au-CeO₂_H sample. In view of these facts, we concluded that the higher selectivity of Au-CeO₂_N to benzoic acid may result from longer diffusion time of reactants within the pore network of Au-CeO₂_N sample. It is highly probable that the longer diffusion pathway observed for Au-CeO₂_N sample promoted further oxidation of the primary product of the alcohol oxidation, i.e., benzaldehyde, to benzoic acid. As far as the selectivity is concerned, it is worth noting that gold nanoparticles formed on the surface of Au-CeO₂_N were significantly smaller than those found in Au-CeO₂_H. Taking this fact into account, we assert that high selectivity of the former catalyst to benzoic acid may result not only from the differences in porosity of these two catalysts, but also to some extent, from the differences in gold particle size. It is highly probable that smaller gold nanoparticles found in Au-CeO₂_N exhibited stronger ability to chemisorb benzaldehyde than the larger ones observed for Au-CeO₂_H, and this promoted further oxidation of this primary product to benzoic acid.

4. Materials and Methods

4.1. Materials

The reagents were cerium(III) nitrate hexahydrate (Sigma-Aldrich; 99.99%), gold(III) chloride hydrate (Sigma-Aldrich, Saint-Louis, MI, USA; 99.995%), hexamethylenetetramine (Sigma-Aldrich, Saint-Louis, MI, USA; ≥99.5%), urea (Fluka, Monte Carlo; ≥99%); sodium hydroxide (POCH; analytical grade), benzyl alcohol (Sigma-Aldrich, Saint-Louis, MI, USA; 99.8%), methanol (HPLC grade; Sigma-Aldrich), deionized water. All the reagents were used without any further purification.

4.2. Synthesis of Catalysts

In a typical synthesis, 14.99 mmol (6.51 g) of cerium(III) nitrate hexahydrate was dissolved in 150 mL of deionized water. At the same time, 0.789 mmol (0.2682 g) of gold(III) chloride hydrate was dissolved in 40 mL of water and then added to the water solution of cerium source upon intensive stirring. In the next step, the as-prepared mixture containing cerium and gold sources was poured into a polypropylene bottle (of total volume = 500 mL). No precipitation at this step of the synthesis was observed. Next, 89.99 mmol of the co-precipitation agent (namely NaOH, urea or HMTA) was dissolved in 150 mL of deionized water and added upon continuous stirring to the propylene bottle containing water solution of cerium and gold sources. At this step, immediate precipitation was observed only for the synthesis with the use of NaOH. In the reaction mixtures containing HMTA and urea, no precipitate was observed to form. Then, the propylene bottle was tightly closed and transferred into the furnace heated to 90 °C. Following the heating for 18 h at 90 °C, the reaction mixture was cooled to room temperature, filtered and washed with water. The as-prepared powder was then dried at 80 °C for 20 h, crushed in a agate mortar and calcined at 400 °C for 2 h (temperature ramp: 1.66 °C/min) followed by calcination at 600 °C for 4 h (temperature ramp: 3.33 °C/min). The gold catalysts prepared with the use of NaOH, HMTA and urea as co-precipitation agents were labelled as Au-CeO₂_N, Au-CeO₂_H and Au-CeO₂_U, respectively. Cerium oxides without gold have been also prepared to be reference materials. In the synthesis of these materials no

gold source was added to the reaction mixture. The concentration of the other reagents was the same as that used for the preparation of Au-CeO₂ catalysts. The as-prepared ceria supports synthesized with the use of NaOH, HMTA and urea were denoted as CeO₂_N, CeO₂_H and CeO₂_U, respectively.

4.3. Characterization of Materials

The as-prepared materials were characterized with the use of inductively coupled plasma-optical emission spectroscopy (ICP-OES), X-ray diffraction measurements (XRD), low-temperature nitrogen adsorption-desorption, transmission electron microscopy (TEM), scanning electron microscopy (SEM), diffuse reflectance ultraviolet-visible spectroscopy (DR UV-vis) and X-ray photoelectron spectroscopy (XPS). Detailed experimental conditions are described in Supplementary Data.

4.4. Catalytic Activity Test

Oxidation of benzyl alcohol was performed using EasyMax 102 Advanced Thermostat system (Mettler Toledo). In a typical reaction, 20 mg of catalyst was added to a glass reactor (total volume of 25 mL) containing a mixture consisted of deionized water (10 mL), benzyl alcohol (20 µL) and sodium hydroxide (390 µL of 0.5 M water solution). The reaction mixture was then tightly closed in the reactor using a septum and purged with oxygen. Following the purging step, a balloon filled with oxygen was connected to the reaction vessel via a needle. Next, the reactor was placed into the EasyMax 102 Advanced Thermostat system and heated to 40 °C under continuous stirring (800 RPM; heating time from room temperature to 40 °C = 5 min). After a given reaction time (20, 40, 80 or 120 min), the reaction mixture was cooled down to 25 °C in five minutes, and then the agitation was stopped. Quantitative analyses of the reaction mixtures were made by high performance liquid chromatography (HPLC). The analysis was carried out using HPLC chromatograph (Waters) equipped with a photodiode array detector (Waters 996). Before the analysis the catalyst was removed from the reaction mixture by filtration through a 0.2 µm Millipore filter. The reactant and the products were separated on an XBridge[®] C18 Column (5 µm, 4.6 × 250 mm, Waters). The eluent was a mixture of methanol and water (vol. ratio of 48/52). In all the reactions carbon mass balance was equal to or higher than 95%.

5. Conclusions

Results obtained in this study clearly show that the type of co-precipitation agent has a significant impact on the structure, texture and catalytic properties of Au-CeO₂ catalysts. It was found that the co-precipitation agent plays an important role in controlling the growth of gold particles. Immediate co-precipitation and growth of Au and CeO₂ in the presence of NaOH was found to be more beneficial for formation of smaller and more uniform gold nanoparticles than gradual co-precipitation and growth of Au-CeO₂ nanostructures in the presence of HMTA or urea. Nevertheless, taking into account relatively large gold particle size observed for the sample prepared with the use of sodium hydroxide as a co-precipitation agent (ca. 12.5 nm in diameter), one can conclude that further research aimed at optimization of synthesis conditions to obtain significantly smaller Au NPs in Au-CeO₂_N nanocomposite is needed.

As concerns the catalysts activity, detailed analysis of the relationship between the properties of gold catalysts supported on cerium dioxide and their catalytic performance allowed drawing a conclusion that the activity of gold catalysts in low-temperature oxidation of benzyl alcohol is strongly affected by the size of gold nanoparticles. The presence of small metallic gold nanoparticles was a key factor for the obtainment of high activity in low-temperature oxidation of benzyl alcohol. It is expected that the new knowledge on the relationship between the type of co-precipitation agent used during the synthesis of Au-CeO₂ catalysts and the properties of the as-synthesized materials may have a significant impact on design and development of new, more active and selective catalysts dedicated

to low-temperature oxidation of alcohols using molecular oxygen as environmentally friendly oxidant.

Supplementary Materials: The following are available online at <https://www.mdpi.com/article/10.3390/catal11050641/s1>, Extended experimental section—Characterization of materials; Figure S1. HRTEM image (a) and SAED diffraction pattern (b) of sample CeO₂-N. In the inset the interplanar distance between 111 planes is denoted; Figure S2. HRTEM image (a) and SAED diffraction pattern (b) of sample CeO₂-H. In the inset the interplanar distance between 111 planes is denoted; Figure S3. HRTEM image (a) and SAED diffraction pattern (b) of sample CeO₂-U.

Author Contributions: Conceptualization, L.W.; methodology, L.W. and G.N.; validation, L.W. and G.N.; investigation, L.W. and G.N.; resources, M.Z. and S.J.; data curation, L.W. and G.N.; writing—original draft preparation, L.W. and G.N.; writing—review and editing, L.W., M.Z. and S.J.; visualization, L.W. and G.N.; supervision, M.Z. and S.J.; funding acquisition, L.W. All authors have read and agreed to the published version of the manuscript.

Funding: This research was funded by the National Science Centre, Poland, grant number 2018/28/C/ST5/00255.

Institutional Review Board Statement: Not applicable.

Informed Consent Statement: Not applicable.

Data Availability Statement: The data presented in this study are available on request from the corresponding author.

Conflicts of Interest: The authors declare no conflict of interest.

References

1. Di Sarli, V.; Landi, G.; Di Benedetto, A.; Lisi, L. Synergy Between Ceria and Metals (Ag or Cu) in Catalytic Diesel Particulate Filters: Effect of the Metal Content and of the Preparation Method on the Regeneration Performance. *Top. Catal.* **2021**, *64*, 256–269. [CrossRef]
2. Cui, Y.; Dai, W.-L. Support morphology and crystal plane effect of Cu/CeO₂ nanomaterial on the physicochemical and catalytic properties for carbonate hydrogenation. *Catal. Sci. Technol.* **2016**, *6*, 7752–7762. [CrossRef]
3. Wang, B.; Zhang, H.; Xu, W.; Li, X.; Wang, W.; Zhang, L.; Li, Y.; Peng, Z.; Yang, F.; Liu, Z. Nature of Active Sites on Cu–CeO₂ Catalysts Activated by High-Temperature Thermal Aging. *ACS Catal.* **2020**, *10*, 12385–12392. [CrossRef]
4. Grabchenko, M.; Mikheeva, N.; Mamontov, G.; Salaev, M.; Liotta, L.; Vodyankina, O. Ag/CeO₂ Composites for Catalytic Abatement of CO, Soot and VOCs. *Catalysts* **2018**, *8*, 285. [CrossRef]
5. Negi, K.; Umar, A.; Chauhan, M.S.; Akhtar, M.S. Ag/CeO₂ nanostructured materials for enhanced photocatalytic and antibacterial applications. *Ceram. Int.* **2019**, *45*, 20509–20517. [CrossRef]
6. Zhu, X.; He, H.; Li, Y.; Wu, H.; Fu, M.; Ye, D.; Wu, J.; Huang, H.; Hu, Y.; Niu, X. CeO₂-Supported Pt Catalysts Derived from MOFs by Two Pyrolysis Strategies to Improve the Oxygen Activation Ability. *Nanomaterials* **2020**, *10*, 983. [CrossRef] [PubMed]
7. Montini, T.; Melchionna, M.; Monai, M.; Fornasiero, P. Fundamentals and Catalytic Applications of CeO₂-Based Materials. *Chem. Rev.* **2016**, *116*, 5987–6041. [CrossRef] [PubMed]
8. Li, L.; Liu, Y.; Wang, Q.; Zhou, X.; Li, J.; Song, S.; Zhang, H. CeO₂ supported low-loading Au as an enhanced catalyst for low temperature oxidation of carbon monoxide. *CrystEngComm* **2019**, *21*, 7108–7113. [CrossRef]
9. Xiang, Y.; He, J.; Sun, N.; Fan, Y.; Yang, L.; Fang, C.; Kuai, L. Hollow mesoporous CeO₂ microspheres for efficient loading of Au single-atoms to catalyze the water-gas shift reaction. *Microporous Mesoporous Mater.* **2020**, *308*, 110507. [CrossRef]
10. Carltonbird, M.; Eaimsumang, S.; Pongstabodee, S.; Boonyuen, S.; Smith, S.M.; Luengnaruemitchai, A. Effect of the exposed ceria morphology on the catalytic activity of gold/ceria catalysts for the preferential oxidation of carbon monoxide. *Chem. Eng. J.* **2018**, *344*, 545–555. [CrossRef]
11. Ishida, T.; Murayama, T.; Taketoshi, A.; Haruta, M. Importance of Size and Contact Structure of Gold Nanoparticles for the Genesis of Unique Catalytic Processes. *Chem. Rev.* **2020**, *120*, 464–525. [CrossRef] [PubMed]
12. Keshri, K.S.; Spezzati, G.; Ruidas, S.; Hensen, E.J.M.; Chowdhury, B. Role of bismuth on aerobic benzyl alcohol oxidation over ceria polymorph-supported gold nanoparticles. *Catal. Commun.* **2020**, *140*, 106004. [CrossRef]
13. Kepeniene, V.; Stagniunaite, R.; Balčiunaite, A.; Tamašauskaite-Tamašiunaite, L.; Norkus, E. Microwave-assisted synthesis of a AuCeO₂/C catalyst and its application for the oxidation of alcohols in an alkaline medium. *New J. Chem.* **2020**, *44*, 18308–18318. [CrossRef]
14. Dong, Y.; Luo, J.; Li, S.; Liang, C. CeO₂ decorated Au/CNT catalyst with constructed Au–CeO₂ interfaces for benzyl alcohol oxidation. *Catal. Commun.* **2020**, *133*, 1–5. [CrossRef]

15. Bu, Y.; Chen, Y.; Jiang, G.; Hou, X.; Li, S.; Zhang, Z. Understanding of Au-CeO₂ interface and its role in catalytic oxidation of formaldehyde. *Appl. Catal. B Environ.* **2020**, *260*, 118138. [[CrossRef](#)]
16. Xu, Y.; Li, J.; Zhou, J.; Liu, Y.; Wei, Z.; Zhang, H. Layered double hydroxides supported atomically precise Au_n nanoclusters for air oxidation of benzyl alcohol: Effects of size and active site structure. *J. Catal.* **2020**, *389*, 409–420. [[CrossRef](#)]
17. Engel, J.; Schwartz, E.; Catlow, C.R.A.; Roldan, A. The influence of oxygen vacancy and Ce³⁺ ion positions on the properties of small gold clusters supported on CeO_{2-x}(111). *J. Mater. Chem. A* **2020**, *8*, 15695–15705. [[CrossRef](#)]
18. Das, S.; Bhattacharjee, G.; Satpati, B.; Kumar, M.; Deka, S.; Ghosalya, M.K.; Gopinath, C.; Bala, T. Deposition of Au nanoparticles inside porous CeO₂ nanocubes using Langmuir-Blodgett technique. *New J. Chem.* **2018**, *42*, 1379–1386. [[CrossRef](#)]
19. Piella, J.; González-Febles, A.; Patarroyo, J.; Arbiol, J.; Bastús, N.G.; Puntes, V. Seeded-Growth Aqueous Synthesis of Colloidal-Stable Citrate-Stabilized Au/CeO₂ Hybrid Nanocrystals: Heterodimers, Core@Shell, and Clover- And Star-Like Structures. *Chem. Mater.* **2019**, *31*, 7922–7932. [[CrossRef](#)]
20. Sudarsanam, P.; Malleshham, B.; Durgasri, D.N.; Reddy, B.M. Physicochemical and catalytic properties of nanosized Au/CeO₂ catalysts for eco-friendly oxidation of benzyl alcohol. *J. Ind. Eng. Chem.* **2014**, *20*, 3115–3121. [[CrossRef](#)]
21. Chen, Z.; Cao, F.X.; Gao, W.; Dong, Q.C.; Qu, Y.Q. Uniform small metal nanoparticles anchored on CeO₂ nanorods driven by electroless chemical deposition. *Rare Met.* **2020**, *39*, 806–814. [[CrossRef](#)]
22. Baatz, C.; Thielecke, N.; Prüße, U. Influence of the preparation conditions on the properties of gold catalysts for the oxidation of glucose. *Appl. Catal. B Environ.* **2007**, *70*, 653–660. [[CrossRef](#)]
23. Radnik, J.; Wilde, L.; Schneider, M.; Pohl, M.M.; Herein, D. Influence of the precipitation agent in the deposition-precipitation on the formation and properties of Au nanoparticles supported on Al₂O₃. *J. Phys. Chem. B* **2006**, *110*, 23688–23693. [[CrossRef](#)] [[PubMed](#)]
24. Zanella, R.; Giorgio, S.; Shin, C.H.; Henry, C.R.; Louis, C. Characterization and reactivity in CO oxidation of gold nanoparticles supported on TiO₂ prepared by deposition-precipitation with NaOH and urea. *J. Catal.* **2004**, *222*, 357–367. [[CrossRef](#)]
25. Chen, B.B.; Shi, C.; Crocker, M.; Wang, Y.; Zhu, A.M. Catalytic removal of formaldehyde at room temperature over supported gold catalysts. *Appl. Catal. B Environ.* **2013**, *132–133*, 245–255. [[CrossRef](#)]
26. She, P.; Xu, K.; He, Q.; Zeng, S.; Sun, H.; Liu, Z. Controlled preparation and visible light photocatalytic activities of corn cob-like Au-ZnO nanorods. *J. Mater. Sci.* **2017**, *52*, 3478–3489. [[CrossRef](#)]
27. Xu, S.; Wang, Z.L. One-dimensional ZnO nanostructures: Solution growth and functional properties. *Nano Res.* **2011**, *4*, 1013–1098. [[CrossRef](#)]
28. Kolodziejczak-Radzimska, A.; Jesionowski, T.; Kolodziejczak-Radzimska, A.; Jesionowski, T. Zinc oxide-from synthesis to application: A review. *Materials* **2014**, *7*, 2833–2881. [[CrossRef](#)]
29. Md Saad, S.K.; Ali Umar, A.; Ali Umar, M.I.; Tomitori, M.; Rahman, M.Y.A.; Mat Salleh, M.; Oyama, M. Two-Dimensional, Hierarchical Ag-Doped TiO₂ Nanocatalysts: Effect of the Metal Oxidation State on the Photocatalytic Properties. *ACS Omega* **2018**, *3*, 2579–2587. [[CrossRef](#)]
30. Tajizadegan, H.; Heidary, A.; Torabi, O.; Golabgir, M.H.; Jamshidi, A. Synthesis and Characterization of ZnCr₂O₄ Nanospinel Prepared via Homogeneous Precipitation Using Urea Hydrolysis. *Int. J. Appl. Ceram. Technol.* **2016**, *13*, 289–294. [[CrossRef](#)]
31. Shishido, T.; Yamamoto, M.; Li, D.; Tian, Y.; Morioka, H.; Honda, M.; Sano, T.; Takehira, K. Water-gas shift reaction over Cu/ZnO and Cu/ZnO/Al₂O₃ catalysts prepared by homogeneous precipitation. *Appl. Catal. A Gen.* **2006**, *303*, 62–71. [[CrossRef](#)]
32. Rosado, T.F.; Teixeira, M.P.; Moraes, L.C.; da Silva, L.A.; Pontes-Silva, A.V.; Taylor, J.G.; de Freitas, I.C.; de Oliveira, D.C.; Gardener, J.; Solórzano, G.; et al. Synergistic Effect between CeO₂ Nanowires and Gold NPs over the Activity and Selectivity in the Oxidation of Thioanisole. *Appl. Catal. A Gen.* **2021**, 118010. [[CrossRef](#)]
33. Zhang, J.H.; Zhu, T.; Li, N.; Xu, C.W. Glycerol Electrooxidation on Au Supported on Carbon Spheres by Stober Method in Alkaline Medium. *Int. J. Electrochem. Sci.* **2013**, *8*, 9508–9517.
34. Thommes, M.; Kaneko, K.; Neimark, A.V.; Olivier, J.P.; Rodriguez-Reinoso, F.; Rouquerol, J.; Sing, K.S.W. Physisorption of gases, with special reference to the evaluation of surface area and pore size distribution (IUPAC Technical Report). *Pure Appl. Chem.* **2015**, *87*, 1051–1069. [[CrossRef](#)]
35. Liu, L.; Yao, Z.; Liu, B.; Dong, L. Correlation of structural characteristics with catalytic performance of CuO/Ce_xZr_{1-x}O₂ catalysts for NO reduction by CO. *J. Catal.* **2010**, *275*, 45–60. [[CrossRef](#)]
36. Reddy, B.M.; Bharali, P.; Saikia, P.; Park, S.E.; Van Den Berg, M.W.E.; Muhler, M.; Grünert, W. Structural characterization and catalytic activity of nanosized Ce_xM_{1-x}O₂ (M = Zr and Hf) mixed oxides. *J. Phys. Chem. C* **2008**, *112*, 11729–11737. [[CrossRef](#)]
37. Aboukaïs, A.; Skaf, M.; Hany, S.; Cousin, R.; Aouad, S.; Labaki, M.; Abi-Aad, E. A comparative study of Cu, Ag and Au doped CeO₂ in the total oxidation of volatile organic compounds (VOCs). *Mater. Chem. Phys.* **2016**, *177*, 570–576. [[CrossRef](#)]
38. Corro, G.; Cebada, S.; Pal, U.; Fierro, J.L.G. Au⁰-Au³⁺ bifunctional site mediated enhanced catalytic activity of Au/ZnO composite in diesel particulate matter oxidation. *J. Catal.* **2017**, *347*, 148–156. [[CrossRef](#)]
39. Villa, A.; Dimitratos, N.; Chan-Thaw, C.E.; Hammond, C.; Veith, G.M.; Wang, D.; Manzoli, M.; Prati, L.; Hutchings, G.J. Characterisation of gold catalysts. *Chem. Soc. Rev.* **2016**, *45*, 4953–4994. [[CrossRef](#)]
40. Pereira, A.; Blouin, M.; Pillonnet, A.; Guay, D. Structure and valence properties of ceria films synthesized by laser ablation under reducing atmosphere. *Mater. Res. Express* **2014**, *1*, 015704. [[CrossRef](#)]

-
41. Ismail, A.A.; Harraz, F.A.; Faisal, M.; El-Toni, A.M.; Al-Hajry, A.; Al-Assiri, M.S. A sensitive and selective amperometric hydrazine sensor based on mesoporous Au/ZnO nanocomposites. *Mater. Des.* **2016**, *109*, 530–538. [[CrossRef](#)]
 42. Scirè, S.; Liotta, L.F. Supported gold catalysts for the total oxidation of volatile organic compounds. *Appl. Catal. B Environ.* **2012**, *125*, 222–246. [[CrossRef](#)]